



**Representing
hydrodynamic
features from lidar
topography**

B. R. Hodges

Representing hydrodynamically-important blocking features in coastal or riverine lidar topography

B. R. Hodges

Department of Civil, Architectural, and Environmental Engineering, The University of Texas at Austin, Austin, Texas, USA

Received: 1 December 2014 – Accepted: 2 February 2015 – Published: 13 February 2015

Correspondence to: B. R. Hodges (hodges@utexas.edu)

Published by Copernicus Publications on behalf of the European Geosciences Union.

Title Page

Abstract

Introduction

Conclusions

References

Tables

Figures



Back

Close

Full Screen / Esc

Printer-friendly Version

Interactive Discussion



Abstract

New automated methods are developed for identifying narrow landscape features that cause hydrodynamic blocking and might have critical impacts for management models of river flooding, coastal inundation, climate change, or extreme event analysis. Lidar data processed into a fine-resolution raster (1 m × 1 m) can resolve narrow blocking features in topography, but typically cannot be directly used for hydrodynamic modeling. For practical applications such data are abstracted to larger scales, which can result in a loss of hydrodynamic blocking effects. The traditional approach to resolving hydrodynamic blocking features is to represent them as cell boundaries within customized unstructured grid that is tuned to the spatial features. A new automated edge-blocking approach is developed, which allows application of an arbitrary structured (Cartesian) mesh at coarser scales and provides contiguous representation of blocking features along Cartesian cell boundaries. This approach distorts the shape of a blocking feature (i.e., making it rectilinear along grid cell faces), but retains its critical hydrodynamic blocking height characteristics and spatial continuity within the topographic model.

1 Introduction

Hydrodynamic models are useful tools for exploring how climate change, rising sea levels, and hydrological regime alterations might affect the interaction between tides, rivers and coastlines (Purvis et al., 2008; Bhuiyan and Dutta, 2012; Nardin and Edmonds, 2014), as well as urban coastal flooding (Gallien et al., 2013; Webster et al., 2014). Similarly, such models are vital in analysis of river hydrodynamics and floodplain inundation that might be affected by changing climate patterns (Wen et al., 2013; Vastila et al., 2010). Unfortunately, modeling annual to decadal timescales for management and climate change analyses typically requires hydrodynamic model grid scales that might not adequately represent narrow blocking features. Herein we develop new

NHESSD

3, 1427–1452, 2015

Representing hydrodynamic features from lidar topography

B. R. Hodges

Title Page

Abstract

Introduction

Conclusions

References

Tables

Figures



Back

Close

Full Screen / Esc

Printer-friendly Version

Interactive Discussion



methods for upscaling a digital elevation model of topography to ensure hydrodynamic blocking features are retained.

The working hypothesis of this paper is that at any sufficiently coarse grid scale (ΔC) there might be topographic features of width scale $\ell_W < \Delta C$ and length scale $\ell_L \geq \Delta C$ that can be represented as “edge” or “face” features of the grid cell. These features, if given the correct continuity across multiple grid cells, can represent hydrodynamic blocking that is lost when subgrid features are represented as topographic roughness. We will call this an *edge blocking* technique.

By way of background, the present state-of-the-art for processed lidar data can readily provide $\sim 1 \text{ m} \times 1 \text{ m}$ topography for use in high-resolution hydrodynamic modeling (Schubert et al., 2008; Sampson et al., 2012). Unfortunately, modeling at such fine spatial resolution invariably drives the model time step down to one second or lower, depending on the numerical model scheme¹. At such scales, even a small river delta of 1000 ha will require $\sim 10^7$ grid cells and $\sim 10^7$ time steps per year of simulation – pushing even a small system into supercomputer territory for multi-decadal and/or Monte Carlo simulations for sensitivity analyses, which are desirable for adaptive coastal management. However, by coarsening to a $20 \text{ m} \times 20 \text{ m}$ grid resolution, 1000 hectares requires only 2.5×10^4 grid cells and can typically be run at time steps of 10 to 30 s in a semi-implicit model², i.e., $\sim 10^6$ time steps per year of simulation. The reduced memory requirement allows multiple model instances to be simultaneously run on a standard multi-core desktop workstation. The larger allowable time step allows faster simulations over longer timescales without requiring extensive high-end computational resources. Indeed, it is likely that as computers get more powerful, our desire to decrease grid resolution will be countered by our desire to run larger areas and longer timescale simulations. Thus, the need for grid coarsening of lidar data for

¹The BreZo code of Sanders et al. (2010) required time steps of 0.05 s for 0.8 m triangular mesh in Schubert et al. (2008).

²Depending on the hydrodynamic discretization and the typical flow velocities.

Representing hydrodynamic features from lidar topography

B. R. Hodges

Title Page

Abstract

Introduction

Conclusions

References

Tables

Figures

◀

▶

◀

▶

Back

Close

Full Screen / Esc

Printer-friendly Version

Interactive Discussion



hydrodynamics is unlikely to disappear, and the challenge we face is in upscaling the topography while capturing the hydrodynamic effects of unresolved features.

As an alternative to grid coarsening, grid nesting (from fine to coarse grids) can be applied to somewhat reduce computational costs (e.g., Webster et al., 2014), but such methods inherently require an expert modeler to make a judgement as to where model resolution might be coarsened. Artificial porosity approaches seem appropriate for urban areas with multiple pathways around unresolved objects (Sanders et al., 2008), but it is not clear that they are necessarily useful in broader natural settings or where narrow objects are blocking over multiple cells. Quadtree subgrid nesting for hydrodynamic models appears to be one approach for upscaling effects of fine-resolution topography without resorting to edge features (Stelling, 2012; Volp et al., 2013), but such methods are still in the early stages of development and cannot be considered a definitive solution. Indeed, it is not clear that simple application of quadtree methods would necessarily preserve contiguous blocking edges, so combining quadtree with the present edge blocking technique might be necessary.

Upscaling of lidar data presents hydrodynamic modeling challenges (Fewtrell et al., 2008). Prior to lidar, our topographic data was generally coarser than model grid scales (Bates, 2004), so translating topography to a model grid was a matter of simple interpolation from a sparse data set and calibrating roughness for effects of unknown features. With the advent of lidar, as noted by Bates et al. (2003) “we need methods to identify and connect linear topographic features . . . given their significant hydraulic impact.” Despite more than 75 citations of this pioneering work, the challenge of *identifying and connecting linear topographic features* has not been addressed in the past decade, and thus provides the fundamental motivation for the present work. Herein we present a new method for identifying, extracting, and representing topographic features that extend over multiple coarse-grid cells, but are so narrow that their hydrodynamic blocking effects would be lost in common upscaling techniques.

As a simple example of the challenge, consider the satellite photograph and corresponding lidar data in Fig. 1a and b, which show a portion of a railroad dike that cuts

NHESSD

3, 1427–1452, 2015

Representing hydrodynamic features from lidar topography

B. R. Hodges

Title Page

Abstract

Introduction

Conclusions

References

Tables

Figures

◀

▶

◀

▶

Back

Close

Full Screen / Esc

Printer-friendly Version

Interactive Discussion



NHESSD

3, 1427–1452, 2015

Representing hydrodynamic features from lidar topography

B. R. Hodges

Title Page

Abstract

Introduction

Conclusions

References

Tables

Figures

◀

▶

◀

▶

Back

Close

Full Screen / Esc

Printer-friendly Version

Interactive Discussion



across the Nueces River delta in Texas, USA, just outside the City of Corpus Christi. The dike is approximately 5 m across at the top and 15 m across at the base. If the lidar data is rasterized a to 20 m × 20 m grid using a simple arithmetic mean of the finer scale data (Fig. 1c), the dike loses both its overall blocking height and continuity. A hydrodynamic model using this coarser grid would have flow paths through the dike at 1.5 to 2 m a.s.l. rather than being contiguously blocked at a 3 m elevation.

Where dikes, embankments, and complex topography are narrower than a practical hydrodynamic grid, the traditional solution has been use of unstructured grids designed with cell boundaries coincident to narrow blocking features (e.g., Cobby et al., 2003; Tsubaki and Fujita, 2010). Unfortunately, unstructured grids usually require significant expertise and “hands-on” artistry to develop an acceptable balance between hydrodynamic modeling practicality and fidelity to the physical topography (Schubert et al., 2008; Mandlburger et al., 2009). As another approach, Ryan and Hodges (2011) modeled the 7500 hectares of the Nueces River delta with a structured Cartesian grid where the narrow railroad dike across the delta (Fig. 1) was represented as an elevated edge feature in a 2-D hydrodynamic model. Identifying this contiguous edge feature on the raster grid was a labor-intensive manual task, but was critical to obtaining the correct hydraulic blocking effects.

It can be stated without reservation that hydrodynamic modeling is simpler if a single size and shape of grid element is used across an entire domain. Such a grid might be called an “arbitrary” grid as, by definition, it is not tuned to match any particular topographic feature. The problem with arbitrary grids is that at coarse resolution they will not have the proper connectivity of either narrow flow paths or narrow blocking structures. Thus, the simplicity of arbitrary gridding does not necessarily imply a better model. However, if narrow blocking features can be upscaled to the edges of the arbitrary grid cells and the correct continuity preserved over multiple cells, then the feature’s effect on flow blocking can be retained, albeit at some distortion of the shape and location of the object. However, such distortions are inherently at the model grid scale, and hence should be acceptable for a coarse-grid model.

Representing hydrodynamic features from lidar topography

B. R. Hodges

Title Page

Abstract

Introduction

Conclusions

References

Tables

Figures



Back

Close

Full Screen / Esc

Printer-friendly Version

Interactive Discussion



For an arbitrary gridding approach to actually simplify modeling, the definition of the coarse-grid edge blocking must be automatic – else we are back to treating grid definition as a labor-intensive art form. This paper introduces a “hands-off” topographic feature extraction system that provides automated identification and representation of fine-scale topographic features that are hydrodynamically important blockages at coarser scales. This new approach captures both the obvious large-scale features (such as the railroad dike) as well as smaller features that are more difficult to identify but might have hydrodynamic blocking influences that are lost in traditional upscaling algorithms. The new approach uses Cartesian grids that are relatively easy to create, modify, and hydrodynamically model. Although unstructured grids have been popular over the past two decades as a way to direct computational power at specifically desired scales, one can make the argument that continually increasing computer power will eventually lead to a return to structured grid modeling that provides simpler automation, requires less expertise in model development, and easier communication between models. It should be noted that this edge blocking concept could also be applied to an arbitrary unstructured grid, however, the object identification and parsing techniques herein rely heavily on the Cartesian structure of the coarse grid to provide simple algorithms.

This paper provides a set of methods to represent fine-scale topographic data in a manner that allows effective hydrodynamic modeling of blocking features at coarser scales on a Cartesian grid. Full implementation and testing of these ideas requires a hydrodynamic model that discriminates between elevations of the grid cell center and elevations of the grid cell faces, which is typically not difficult to include (e.g., Casulli and Cheng, 1992). However, the impact of these new face blocking techniques on the hydrodynamic solution is a subject for future investigations, and will not be addressed herein.

2 Methods

The goal of our lidar processing is to produce a coarse Cartesian grid at some scale $\Delta C > \Delta F$ that retains valuable hydrodynamic characteristics associated with contiguous blockage features (e.g., the railroad dike in Fig. 1). In a conventional Cartesian raster grid, each cell has a single piece of data: the landscape elevation. However, for the coarse grid we will store a representative value for the elevation over the bulk of the grid cell and separate blocking elevation values on each cell face. For convenience in data processing, we will limit our focus to systems where the coarse-to-fine raster ratio $R_\Delta = \Delta C / \Delta F$ is an integer. For sufficiently fine resolution lidar data, this is not a significant limitation. It follows that the coarse-grid raster is of size $n_{cx} \times n_{cy}$, where $n_{cx} = n_{fx} / R_\Delta$ and $n_{cy} = n_{fy} / R_\Delta$, with n_{fx} and n_{fy} as the number of fine-grid cells in the data set (this generally requires truncating some fine-grid data at edges to ensure integral values for n 's). For simplicity in exposition, we will confine ourselves to the case where the x and y directions are resolved with the same R_Δ , although the method is readily extensible to rectangular vice square grid cells.

The general procedure for data processing is:

1. create a fine-grid background topography (Fig. 1d);
2. create a coarse-grid representation of background topography (Fig. 2a);
3. compute the difference between fine and coarse topography (Fig. 2b);
4. identify contiguous objects that occur in the difference set (Fig. 3);
5. identify blocking objects and assign elevations to grid cell faces (Fig. 4).

2.1 Fine-scale background topography

The first step is to separate unresolvable topographic features (at coarse scale ΔC) from a background topography, i.e., estimating what the fine-scale landscape would

Representing hydrodynamic features from lidar topography

B. R. Hodges

Title Page

Abstract

Introduction

Conclusions

References

Tables

Figures



Back

Close

Full Screen / Esc

Printer-friendly Version

Interactive Discussion



look like with coarse-scale unresolvable features removed. Herein we apply a *median filter*, which was originally designed for image noise removal but has proven more widely useful, e.g., removing the signature of large woody debris from bathymetric data (White and Hodges, 2005). A median filter replaces the value at position (x, y) with the median of the values in some neighborhood around the point; the neighborhood size is defined as the filter size. The filter operation is accomplished on a moving window over the fine-scale grid to produce a smooth rendition of the background elevations that are resolvable at a coarser resolution; that is, the original resolution of the data set is maintained (e.g., unlike the averaging in Fig. 1c) while the unresolvable features are removed. For example, the $1\text{ m} \times 1\text{ m}$ lidar data is processed with different size median filters as shown in Fig. 1d–f, providing smooth, high-resolution background elevations.

Clearly, the filter scale for defining background topography should be equal to or greater than the desired coarse-grid scale. If the median filter is smaller than the coarse grid, then objects that cannot be resolved will remain in the filtered data set, and hence not in the difference data set (see below). Indeed, it seems prudent to generally apply a median filter that is twice the desired coarse-grid scale to ensure that the data set is sufficiently smooth for hydrodynamic modeling. That is, if a $20\text{ m} \times 20\text{ m}$ coarse grid is desired and a $20\text{ m} \times 20\text{ m}$ median filter is applied, there can be features slightly larger than 20 m that will appear across two coarse grid cells and hence will not really be hydrodynamically resolved. This effect is clear in Fig. 1f, where the $20\text{ m} \times 20\text{ m}$ filter shows a partial signature of the railroad dike that would be lost in upscaling to the coarse grid as in Fig. 1c.

2.2 Coarse background and difference data set

The median filtered fine-scale data, Fig. 1d, is used to produce a coarse-grid approximation of the landscape elevation, Fig. 2a. This step can be accomplished using either the simple arithmetic mean or median of elevations inside the coarse grid cell (herein the median is used). This coarse-grid representation is pushed back to the fine grid

Representing hydrodynamic features from lidar topography

B. R. Hodges

Title Page

Abstract

Introduction

Conclusions

References

Tables

Figures



Back

Close

Full Screen / Esc

Printer-friendly Version

Interactive Discussion



(i.e., using identical values for all the fine cells within a single coarse-grid cell) so that a fine-scale difference map can be created (Fig. 2b).

2.3 Identification of objects

The difference map contains both negative objects (unresolved depressions) and positive objects (unresolved blockages). The present work focusses on the positive objects³ that are relatively easy to handle in a hydrodynamic model that includes cell edge elevations. To identify blocking positive objects, a cutoff height (Δh) is specified above which an object is deemed a hydrodynamic blockage rather than simply topographic roughness. The number and size of objects will be a function of this cutoff. For the present demonstration, the cutoff height is $\Delta h = 0.2$ m. A binary data set can be defined as $\{0,1\}$ based on whether fine-grid cells are respectively below or above Δh , as shown in Fig. 3a. The binary data can be manipulated using *bwmorph* and *bwboundaries* in the Matlab Image Processing Toolbox. The *bwmorph* function, through its “clean” option, identifies isolated pixels in a binary image and removes them – an image noise removal operation. The *bwboundaries* function uses the Moore-Neighbor tracing algorithm (Gonzalez et al., 2004) to identify individual objects that are formed by contiguous pixels and unconnected to other objects, as shown in Fig. 3b. Herein, the “noholes” option of *bwboundaries* is used to remove any depressions in the center of objects.

For the present work, it is also useful to remove objects that are too small to block a coarse grid cell; i.e., for a $20\text{ m} \times 20\text{ m}$ coarse grid based on a $1\text{ m} \times 1\text{ m}$ data set ($R_\Delta = 20$), any object in Fig. 3a that consists of less than $N_c = 20$ fine-grid cells cannot hydraulically block a coarse-grid cell, and can be excised from the object data set. To allow some flexibility, it is useful to define the removal criterion as $N_c \leq R_\Delta - \delta$, where

³Note that negative objects are fine-scale flow paths that are not represented within the coarse-grid topography and are an important subject for further research.

Representing hydrodynamic features from lidar topography

B. R. Hodges

Title Page

Abstract

Introduction

Conclusions

References

Tables

Figures

◀

▶

◀

▶

Back

Close

Full Screen / Esc

Printer-friendly Version

Interactive Discussion



$\delta \in \{0, 1, 2, \dots\}$ is a user-defined parameter that allows nearly blocking objects ($\delta > 0$) to be retained in the object data set. Herein $\delta = 1$ is used.

2.4 Snap-grid object blocking

Each object can be processed separately to provide hydraulic blocking conditions on both row and column faces of a coarse grid cell. A typical object and its elevations (Fig. 4a) has a binary representation at the fine-grid level, as shown in Fig. 4b. Let $f_o(x_c, y_c)$ be the set of fine-grid cells of the object, where x_c and y_c are coordinates measured relative to the coarse grid. The coarse grid demarcation lines are, by definition, integer values in our coarse-grid numbering scheme. This is perhaps slightly unconventional for hydrodynamic modelers as the coarse-grid cell centers are therefore at non-integer values, i.e., the location $(x_c, y_c) = (i - 1/2, j - 1/2)$ defines a coarse-grid cell in the raster set for $i = \{1, 2, 3, \dots, n_{cx}\}$, $j = \{1, 2, 3, \dots, n_{cy}\}$ with faces at coarse-grid indexes $(x_c, y_c) \in \{(i, j - 1/2), (i - 1, j - 1/2), (i - 1/2, j), (i - 1/2, j - 1)\}$. Using this indexing, we can define $G_y(i - 1/2, j) = f_o(x_c, \text{round}(y_c))$ as a set of fine-grid cells of varying x_c that are “snapped” to an integer y_c face (the red \times markers in Fig. 4c). Similarly $G_x(i, j - 1/2) = f_o(\text{round}(x_c), y_c)$ is the set of blocking cells of varying y_c snapped to an integer x_c face, (the blue $+$ markers in Fig. 4c). For the purposes of determining whether or not blocking occurs, the cells sets G_x and G_y are true mathematical sets that do not include duplicate values. However, data sets with duplicates (denoted as G_{yy} and G_{xx}) are retained for computation of blocking height (discussed below).

To determine *snap-grid blocking* of coarse grid faces (Fig. 4d), the sizes of set $G_y(i - 1/2, j)$ and $G_x(i, j - 1/2)$ are defined as $N_y(i - 1/2, j)$ and $N_x(i, j - 1/2)$, respectively. These are the number of unique values of x_c on a $\text{round}(y_c)$ face (red \times markers on a column face) and the number of unique y_c values on a $\text{round}(x_c)$ face (blue $+$ markers on a row face). Snap-grid blocking occurs along coarse-grid column faces that satisfy

$$N_y(i - 1/2, j) \geq R_\Delta - \delta \quad (1)$$

Representing hydrodynamic features from lidar topography

B. R. Hodges

Title Page

Abstract

Introduction

Conclusions

References

Tables

Figures

◀

▶

◀

▶

Back

Close

Full Screen / Esc

Printer-friendly Version

Interactive Discussion



and coarse-grid row faces that satisfy

$$N_x(i, j - 1/2) \geq R_\Delta - \delta \quad (2)$$

where δ is the same $\delta \in \{0, 1, 2, \dots\}$ used for identifying objects (above). Note that this approach allows the fine cells to serve both as blocking in the x and y directions simultaneously, which is necessary to represent the hydraulic blocking of objects at an angle to the coarse grid. After a face is blocked, e.g., as shown in Fig. 4d, the corresponding $G_y(i - 1/2, j)$ and $G_x(i, j - 1/2)$ are set to zero so that fine-grid cells used to define a snap-grid block are not used in computing *cross-cell blocking* (discussed below).

2.5 Small object shift

The snap-grid blocking approach will necessarily depend on the spatial relationship between the objects and the coarse grid. For small objects, a slight shift of the object position can change whether or not the object is judged to be blocking. For example, the lower column face blocking Fig. 4d would not have been identified as blocking in the original object position, shown in Fig. 4a, because some of the fine-grid cells would have shown up in an adjacent column such that Eq. (1) would not have been satisfied for either face. For small objects (less than $1.5\Delta C$), it is convenient to simply shift the object (as in Fig. 4b) to maximize the number of fine-grid blocking cells within a single coarse grid cell. As long as the shift is less than $\Delta C/4$, it does not significantly affect the coarse-grid physical relationships. Object shifting can be accomplished with an automated algorithm that is based on the total extent of a small object and the overhang of the object into adjacent cells.

2.6 Cross-cell object blocking

Depending on an object's topology, the blocked faces determined by the snap-grid approach (described above) might not provide a contiguous blocked path. Consider

Representing hydrodynamic features from lidar topography

B. R. Hodges

Title Page

Abstract

Introduction

Conclusions

References

Tables

Figures

◀

▶

◀

▶

Back

Close

Full Screen / Esc

Printer-friendly Version

Interactive Discussion



Representing hydrodynamic features from lidar topography

B. R. Hodges

Title Page

Abstract

Introduction

Conclusions

References

Tables

Figures

◀

▶

◀

▶

Back

Close

Full Screen / Esc

Printer-friendly Version

Interactive Discussion



the larger object in Fig. 5a, where snap-grid blocking provides the results in Fig. 5b and c. It is clear that some hydraulic blocking has not been captured: the G_x (the blue + markers) and G_y (red × markers) in the second coarse-grid cell from the top do not satisfy Eqs. (1) or (2) as they are split between different faces. Furthermore in the lowermost coarse-grid cell, the red × markers on either face are insufficient for blocking. These effects arise because the snap-grid approach uses rounding, which can split the blocking fine-grid cells to the upper and lower faces of the coarse grid cell. To address this issue, we define a *cross-cell blocking* approach for column and row faces. Cross-cell blocking is conducted after snap-grid blocking and only uses the fine-grid cells that were not applied in snap-grid blocking; e.g., the remaining red × and blue + in Fig. 5c.

For the coarse-grid cell centered at $(i-1/2, j-1/2)$, we define sets of unique fine-grid blocking cells across the cell center as

$$H_y(i-1/2, j-1/2) = G_y(i-1/2, j) \cup G_y(i-1/2, j-1) \quad (3)$$

$$H_x(i-1/2, j-1/2) = G_x(i, j-1/2) \cup G_x(i-1, j-1/2) \quad (4)$$

which are illustrated in Fig. 5d. Blocking conditions are defined similar to Eqs. (1) and (2), using N_y and N_x as the size of the unique H_y and H_x cell sets. For determining object blocking height (discussed below), we also define sets that retain non-unique elements,

$$H_{yy}(i-1/2, j-1/2) = G_{yy}(i-1/2, j) \cup G_{yy}(i-1/2, j-1) \quad (5)$$

$$H_{xx}(i-1/2, j-1/2) = G_{xx}(i, j-1/2) \cup G_{xx}(i-1, j-1/2). \quad (6)$$

As the H_y and H_x fine-cell sets cross the coarse-cell center, face blocking could be at either of the grid cell faces, as shown by dashed blocking lines in Fig. 5d. Indeed, there can be more than one set of blocking faces that provides a reasonable representation of cross-cell blocking. The critical issue is ensuring that cross-cell blocking is contiguous; i.e., there are choices for cross-cell blocking faces in Fig. 5d that would not provide contiguous blocking. The simplest algorithm for selecting blocking is to process column faces (red ◦) and row faces (blue Δ) sequentially. If a coarse cell contains

Representing hydrodynamic features from lidar topography

B. R. Hodges

Title Page

Abstract

Introduction

Conclusions

References

Tables

Figures



Back

Close

Full Screen / Esc

Printer-friendly Version

Interactive Discussion



only a single blocked end point (e.g., the lowermost complete cell in Fig. 5d), then the cross-cell blocked face (either row or column) must connect to that blocked end. If a coarse cell contains two blocked end points, then the algorithm must distinguish between diagonally-blocked points (e.g., the 2nd coarse cell from the top in Fig. 5d) and co-linear blocked end points along a face (either row or column). Where two blocked end points are along a single column face and cell-center blocking for a column face exists (red \circ), the cell-center blocking logically must be along the face that connects the blocked end points. Similarly, where two blocked end points are along a row face and cell-center blocking for a row face is indicated (blue Δ), then the blocking is necessarily along the row face connecting the blocked end points. However, where two blocked end points are co-linear along a column face and the cell-centered blocking is indicated for a row face (or vice versa), then the choice of which face to block may be taken arbitrarily. Similarly, when two blocked end points are diagonally opposed, the selection of the blocking face is arbitrary. Note that these arbitrary choices will necessarily set up a condition where three end points are blocked. Because rows and columns are processed sequentially, diagonal blocking of two end points solved using columns (first cycle) sets up a cell with three blocked end points for solving using rows (second cycle). If three end points are blocked, then the cross-cell blocking must connect the two blocked end points that are co-linear along the column or row face (as appropriate), which ensures continuity of the feature.

In the present data set, all the objects achieved contiguous edge-blocking representations using the snap-grid and cross-cell object blocking algorithms outlined above. However, one can imagine a feature that is longer and narrower than shown in Fig. 5 for which the procedure might fail. For a long narrow feature, it is possible that multiple iterations of the cross-cell algorithm would be required to define a blocking condition. That is, the cross-cell algorithm described above combines (for example) the G_x blocking cells of two opposite column faces into a single cell-centered H_x that is tested for blocking. If $H_x < R_\Delta - \delta$ there is no blocking, and one can loop the algorithm to look for larger-scale blocking by combining the H_x of two adjacent cells into a I_x that is evalu-

Representing hydrodynamic features from lidar topography

B. R. Hodges

Title Page

Abstract

Introduction

Conclusions

References

Tables

Figures



Back

Close

Full Screen / Esc

Printer-friendly Version

Interactive Discussion



have not yet developed an automated approach for this task. Once the edge blocking data set is defined, as in Fig. 6b, the start and the end of the bridge section (visually apparent from the change in the width of the dike in Fig. 1b) can be used to identify the edge blocking cells in between. These data are easily removed from the edge cell set – i.e., their values are simply set to “not a number.” That is, where edge blocking is not identifiable, there is no need to store any edge-blocking heights. In theory, this technique might have wider applicability in removing the bridge from the original 1 m × 1 m lidar. It might be possible to trace back the relationship between the bridge edges removed, the pixels that represented this blocking (i.e., G_{xx} , G_{yy} , H_{xx} and H_{yy}), and the difference data set of Fig. 2b so the corresponding bridge pixels in the 1 m × 1 m lidar Fig. 1b can be replaced by their median-filtered values from Fig. 1d.

Although the median filter for a large data set can be computationally expensive, the edge blocking algorithm is otherwise relatively simple and inexpensive. Raw object identification from the binary image (Fig. 3a) provides 3754 individual objects from the 7.5×10^5 pixels; however 2075 of these are single pixel objects that are easily eliminated. Further removing objects where $N_c \leq R_\Delta - \delta$ leaves only 129 objects for processing (Fig. 3b). During the processing steps, only 56 objects were found to be large enough to block any cell faces, and 21 of these blocked only a single cell face. The importance of such single-face blocking should be considered with analysis in hydrodynamic simulations. It may be that such blocking is better represented by roughness coefficients.

A potential area where the edge-blocking method might be expanded is in the estimation of topographic roughness, which has been a subject of extensive prior research (e.g., Abu-Aly et al., 2014; Casas et al., 2010; Dorn et al., 2014; Forzieri et al., 2011; Straatsma and Baptist, 2008). By defining edge features, a portion of the difference between the grid cell elevation and subgrid features can be removed from the roughness estimation; i.e., we could use (i.e., G_{xx} , G_{yy} , H_{xx} and H_{yy}) to remove pixels that have been resolved in to edge features and only consider the remaining pixels in a coarse grid cell as contributing to roughness.

Representing hydrodynamic features from lidar topography

B. R. Hodges

[Title Page](#)[Abstract](#)[Introduction](#)[Conclusions](#)[References](#)[Tables](#)[Figures](#)[Back](#)[Close](#)[Full Screen / Esc](#)[Printer-friendly Version](#)[Interactive Discussion](#)

There are a number of areas in which the present method could be improved. At several places along the railroad dike there are coarse grid cells that are bounded on all sides by edge blocking. This occurs for cells that are almost directly centered on the dike such that the cross-cell blocking method results in blocked faces in all directions.

Arguably, these coarse-grid cell centers should simply be filled in with the average of the blocked cell faces so that they do not appear as artificial depressions. However, in marshlands there might be actual depressions surrounded by blocking topography that should not be simply filled in. Thus, the method could be improved by an algorithm that distinguishes between these two cases. As yet, we have not identified enough candidate depressions in our data set to test such an algorithm.

A key drawback of the present method is the potential for artificial blocking of narrow flow paths. This can occur where two adjacent objects provide blocked edges that are adjacent in the coarse-grid representation but are separated a narrow flow path in the fine-grid representation. Solution to this problem is likely to be found by addressing the key future challenge: identifying preferential flow paths that are unresolved at the coarse grid scale (i.e., the *negative objects* resulting from unresolved depressions). In Fig. 1a, we can clearly see a narrow stream channel on one side of the railroad dike. This channel is entirely absent in the final topography of Fig. 6. Such channels could be readily identified by using the snap-grid and cell-center blocking techniques as “path” techniques for negative objects (i.e., objects determined similar to Fig. 3a, but using a negative Δh for discrimination). However, it is not clear how such objects could be used in present hydrodynamic models. Definition of preferential narrow flow paths that are unresolved within coarse-grid topography remains an area with no clear solution (D’Alpaos and Defina, 2007). However, there are interesting possibilities in 1-D/2-D model such as Viero et al. (2013) that might provide a good starting point. In any case, inversion of the techniques developed above provides a basis for defining preferential flow paths along coarse grid cell edges as a precursor for developing new hydrodynamic modeling techniques.

4 Conclusions

This paper provides automated identification of hydrodynamic blocking features in fine-scale rasterized lidar topography, along with upscaling of the blockage to a coarser raster grid. These techniques could be used for modeling coastal flood inundation at the practical coarse-grid scales necessary for addressing large-scale adaptive management questions, while retaining the blocking effects of fine-scale features that cannot otherwise be captured.

A coarse grid developed with the new *edge blocking* technique could be immediately applied in any number of 2-D and 3-D hydrodynamic models that permit grid cells to use different topographic elevations on different flow faces. Note that because raster topographic data sets with separate face elevations have not been generally available, many hydrodynamic models do not provide for separate cell-face elevation data. Nevertheless, some models could be readily adapted to using such data with minor modifications and new tools for input data manipulation.

Acknowledgements. This work was originally developed during US National Science Foundation Grant No. 710901 and has continued under NSF Grant No. CCF-1331610. Support of the Texas Water Development Board, the Coastal Bend Bays and Estuaries Program, the City of Corpus Christi, and the US Army Corps of Engineers was instrumental in the development of this project. The lidar data for the Nueces River delta was processed to the 1 m × 1 m scale by J. Gibeaut, Texas A & M University – Corpus Christi.

NHESSD

3, 1427–1452, 2015

Representing hydrodynamic features from lidar topography

B. R. Hodges

Title Page

Abstract

Introduction

Conclusions

References

Tables

Figures



Back

Close

Full Screen / Esc

Printer-friendly Version

Interactive Discussion



References

- Abu-Aly, T. R., Pasternack, G. B., Wyrick, J. R., Barker, R., Massa, D., and Johnson, T.: Effects of LiDAR-derived, spatially distributed vegetation roughness on two-dimensional hydraulics in a gravel-cobble river at flows of 0.2 to 20 times bankfull, *Geomorphology*, 206, 468–482, doi:10.1016/j.geomorph.2013.10.017, 2014. 1441
- 5 Bates, P.: Remote sensing and flood inundation modelling, *Hydrol. Process.*, 18, 2593–2597, doi:10.1002/hyp.5649, 2004. 1430
- Bates, P., Marks, K., and Horritt, M.: Optimal use of high-resolution topographic data in flood inundation models, *Hydrol. Process.*, 17, 537–557, doi:10.1002/hyp.1113, 2003. 1430
- 10 Bhuiyan, M. J. A. N., and Dutta, D.: Assessing impacts of sea level rise on river salinity in the Gorai river network, Bangladesh, *Estuar. Coast. Shelf S.*, 96, 219–227, doi:10.1016/j.ecss.2011.11.005, 2012. 1428
- Casas, A., Lane, S. N., Yu, D., and Benito, G.: A method for parameterising roughness and topographic sub-grid scale effects in hydraulic modelling from LiDAR data, *Hydrol. Earth Syst. Sci.*, 14, 1567–1579, doi:10.5194/hess-14-1567-2010, 2010. 1441
- 15 Casulli, V., and Cheng, R. T.: Semiimplicit finite-difference methods for 3-dimensional shallow-water flow, *Int. J. Numer. Meth. Fl.*, 15, 629–648, 1992. 1432
- Cobby, D., Mason, D., Horritt, M., and Bates, P.: Two-dimensional hydraulic flood modelling using a finite-element mesh decomposed according to vegetation and topographic features derived from airborne scanning laser altimetry, *Hydrol. Process.*, 17, 1979–2000, doi:10.1002/hyp.1201, 2003. 1431
- 20 D’Alpaos, L., and Defina, A.: Mathematical modeling of tidal hydrodynamics in shallow lagoons: a review of open issues and applications to the Venice lagoon, *Comput. Geosci.*, 33, 476–496, doi:10.1016/j.cageo.2006.07.009, 2007. 1442
- 25 Dorn, H., Vetter, M., and Hoefle, B.: GIS-based roughness derivation for flood simulations: a comparison of orthophotos, LiDAR and crowdsourced geodata, *Remote Sensing*, 6, 1739–1759, doi:10.3390/rs6021739, 2014. 1441
- Fewtrell, T. J., Bates, P. D., Horritt, M., and Hunter, N. M.: Evaluating the effect of scale in flood inundation modelling in urban environments, *Hydrol. Process.*, 22, 5107–5118, doi:10.1002/hyp.7148, 2008. 1430
- 30

Representing hydrodynamic features from lidar topography

B. R. Hodges

Title Page

Abstract

Introduction

Conclusions

References

Tables

Figures



Back

Close

Full Screen / Esc

Printer-friendly Version

Interactive Discussion



Representing hydrodynamic features from lidar topography

B. R. Hodges

Title Page

Abstract

Introduction

Conclusions

References

Tables

Figures

◀

▶

◀

▶

Back

Close

Full Screen / Esc

Printer-friendly Version

Interactive Discussion



- Forzieri, G., Degetto, M., Righetti, M., Castelli, F., and Preti, F.: Satellite multi-spectral data for improved floodplain roughness modelling, *J. Hydrol.*, 407, 41–57, doi:10.1016/j.jhydrol.2011.07.009, 2011. 1441
- Gallien, T. W., Barnard, P. L., van Ormondt, M., Foxgrover, A. C., and Sanders, B. F.: A parcel-scale coastal flood forecasting prototype for a Southern California urbanized embayment, *J. Coastal Res.*, 29, 642–656, doi:10.2112/JCOASTRES-D-12-00114.1, 2013. 1428
- Gonzalez, R. C., Woods, R. E., and Eddins, S. L.: *Digital Image Processing Using MATLAB*, Pearson Prentice Hall, Upper Saddle River, New Jersey, 2004. 1435
- Mandlburger, G., Hauer, C., Höfle, B., Habersack, H., and Pfeifer, N.: Optimisation of LiDAR derived terrain models for river flow modelling, *Hydrol. Earth Syst. Sci.*, 13, 1453–1466, doi:10.5194/hess-13-1453-2009, 2009. 1431
- Nardin, W. and Edmonds, D. A.: Optimum vegetation height and density for inorganic sedimentation in deltaic marshes, *Nat. Geosci.*, 7, 722–726, doi:10.1038/NGEO2233, 2014. 1428
- Purvis, M. J., Bates, P. D., and Hayes, C. M.: A probabilistic methodology to estimate future coastal flood risk due to sea level rise, *Coast. Eng.*, 55, 1062–1073, doi:10.1016/j.coastaleng.2008.04.008, 2008. 1428
- Ryan, A. and Hodges, B. R.: Modeling Hydrodynamic Fluxes in the Nueces River Delta, Tech. Rep., CRWR Online Report 11-07, Center for Research in Water Resources, University of Texas at Austin, available at: <http://www.crrw.utexas.edu/online.shtml> (last access: 12 February 2015), 2011. 1431
- Sampson, C. C., Fewtrell, T. J., Duncan, A., Shaad, K., Horritt, M. S., and Bates, P. D.: Use of terrestrial laser scanning data to drive decimetric resolution urban inundation models, *Adv. Water Resour.*, 41, 1–17, doi:10.1016/j.advwatres.2012.02.010, 2012. 1429
- Sanders, B. F., Schubert, J. E., and Gallegos, H. A.: Integral formulation of shallow-water equations with anisotropic porosity for urban flood modeling, *J. Hydrol.*, 362, 19–38, doi:10.1016/j.jhydrol.2008.08.009, 2008. 1430
- Sanders, B. F., Schubert, J. E., and Detwiler, R. L.: ParBreZo: a parallel, unstructured grid, Godunov-type, shallow-water code for high-resolution flood inundation modeling at the regional scale, *Adv. Water Resour.*, 33, 1456–1467, doi:10.1016/j.advwatres.2010.07.007, 2010. 1429
- Schubert, J. E., Sanders, B. F., Smith, M. J., and Wright, N. G.: Unstructured mesh generation and landcover-based resistance for hydrodynamic modeling of urban flooding, *Adv. Water Resour.*, 31, 1603–1621, doi:10.1016/j.advwatres.2008.07.012, 2008. 1429, 1431

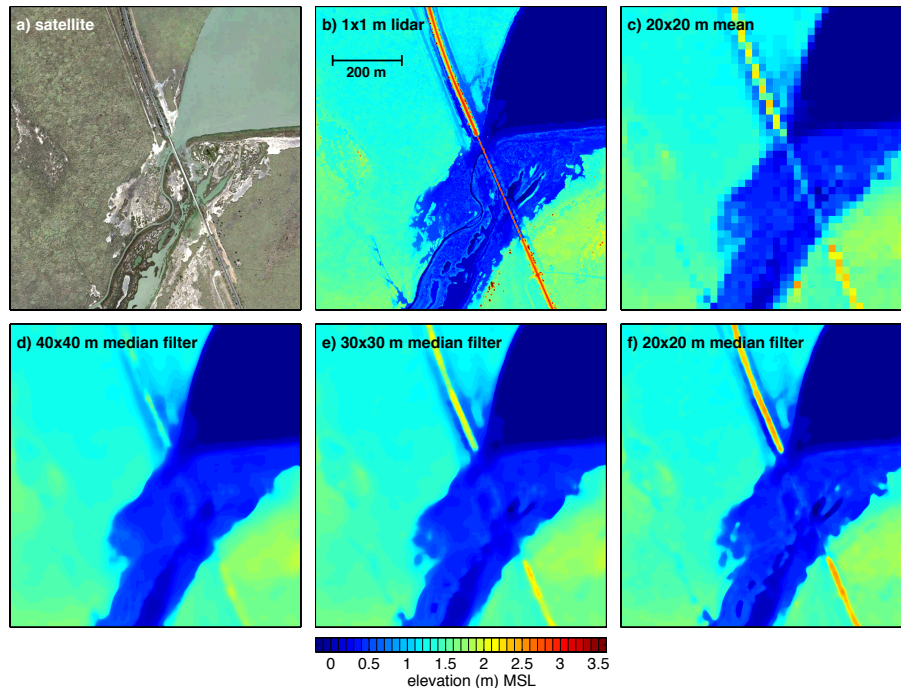


Figure 1. A 75 hectare section of the Rincon Bayou in the Nueces River delta shown in Google Earth satellite photo **(a)**, which is centered at $27^{\circ}53'20''$ N $97^{\circ}34'11''$ W. Comparing the $1\text{ m} \times 1\text{ m}$ resolution lidar data **(b)** courtesy of J. Gibeaut, Texas A&M Corpus Christi, and the arithmetic mean of the data computed on a $20\text{ m} \times 20\text{ m}$ grid **(c)**, illustrates the loss of hydrodynamic blocking height and continuity when a simple mean is used for coarse grid elevations (results for a $20\text{ m} \times 20\text{ m}$ median, not shown, are almost indistinguishable). Frames **(d)** through **(f)** show applications of median filtering (see Methods) with varying filter scales, retaining the original $1\text{ m} \times 1\text{ m}$ resolution but eliminating unresolvable features from the data set.

Representing hydrodynamic features from lidar topography

B. R. Hodges

Title Page

Abstract Introduction

Conclusions References

Tables Figures

◀ ▶

◀ ▶

Back Close

Full Screen / Esc

Printer-friendly Version

Interactive Discussion



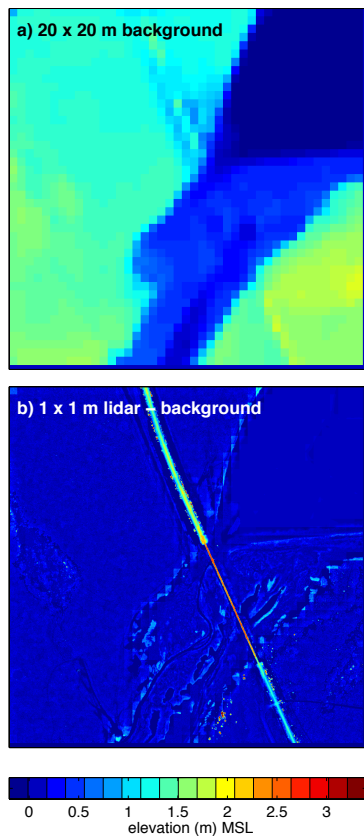


Figure 2. (a) The 20 m \times 20 m coarse-grid background topography based on the 40 m \times 40 m filter of Fig. 1d; and (b) the difference between the 1 m \times 1 m lidar data of Fig. 1b and the coarse-grid background topography.

Representing hydrodynamic features from lidar topography

B. R. Hodges

Title Page

Abstract

Introduction

Conclusions

References

Tables

Figures

◀

▶

◀

▶

Back

Close

Full Screen / Esc

Printer-friendly Version

Interactive Discussion



Representing hydrodynamic features from lidar topography

B. R. Hodges

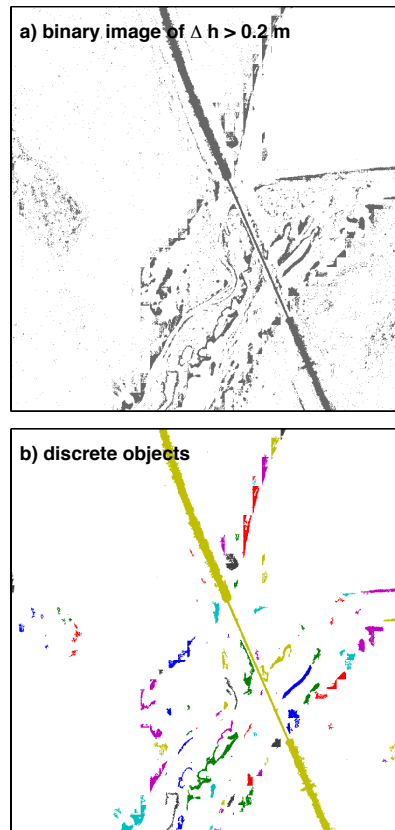


Figure 3. Binary image (a) of difference data set from Fig. 2b, which can be used to identify separate objects, shown in colors in (b). Note that objects smaller than 20 fine-grid cells in (a) have been eliminated in (b).

[Title Page](#)[Abstract](#)[Introduction](#)[Conclusions](#)[References](#)[Tables](#)[Figures](#)[◀](#)[▶](#)[◀](#)[▶](#)[Back](#)[Close](#)[Full Screen / Esc](#)[Printer-friendly Version](#)[Interactive Discussion](#)

Representing hydrodynamic features from lidar topography

B. R. Hodges

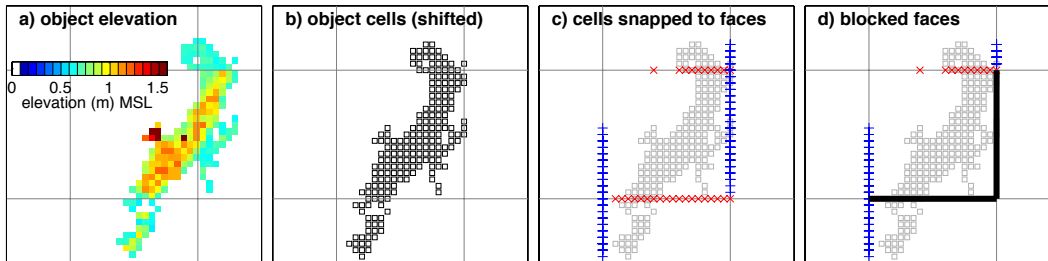


Figure 4. Blocking caused by a small object. The red \times and blue $+$ represent fine-grid blocking cells (gray \square) snapped to the coarse-grid faces G_y and G_x ; black lines are the resulting blocked coarse grid faces. Here and throughout this paper $\delta = 1$ is used for defining blocking. The object cells in (b) are slightly shifted from (a) as discussed in the text to better align with coarse grid.

Title Page

Abstract

Introduction

Conclusions

References

Tables

Figures

◀

▶

◀

▶

Back

Close

Full Screen / Esc

Printer-friendly Version

Interactive Discussion



Representing hydrodynamic features from lidar topography

B. R. Hodges

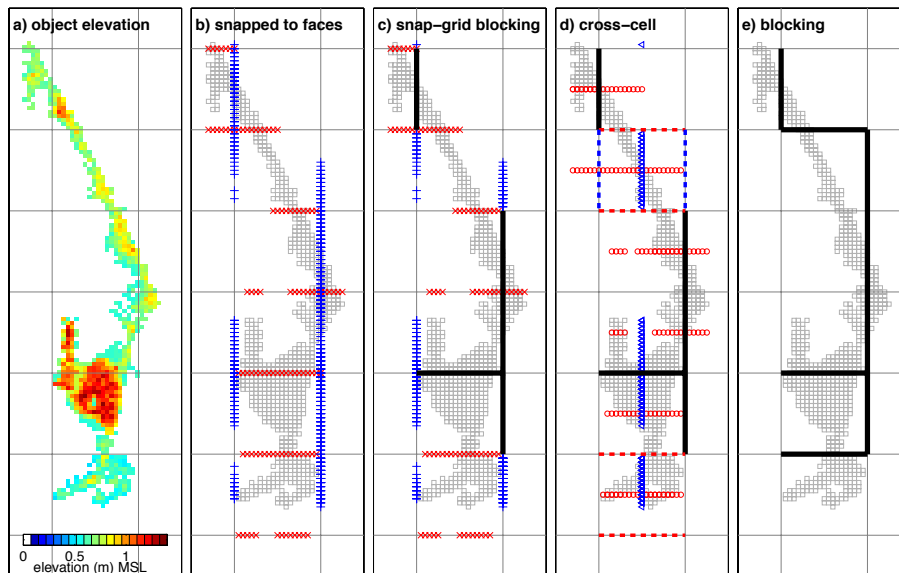


Figure 5. Blocking caused by a large object similar to Fig. 4 for frames (a) through (c). In (d) the remaining G_y and G_x are transformed to cell-center H_y and H_x blocking shown with red \circ and blue Δ , and different possible blocking paths are illustrated with dashed lines; (e) shows final blocking paths that are contiguous.

Title Page

Abstract

Introduction

Conclusions

References

Tables

Figures

◀

▶

◀

▶

Back

Close

Full Screen / Esc

Printer-friendly Version

Interactive Discussion



Representing hydrodynamic features from lidar topography

B. R. Hodges

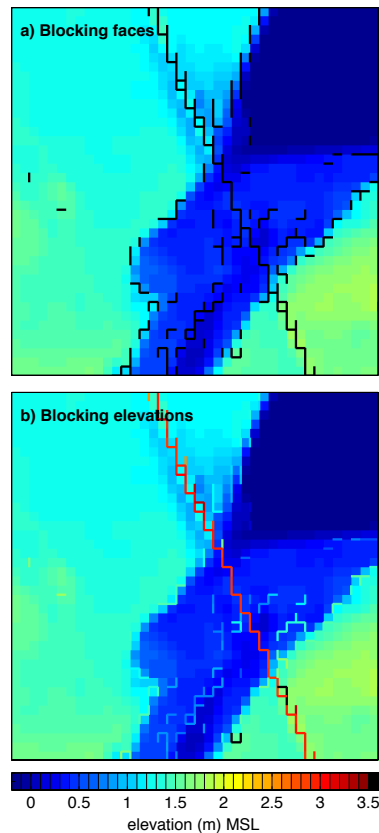


Figure 6. The snap-grid and cell-center blocking methods applied to the median-filtered background topography from Fig. 2. In (a) the locations of all blocked faces are shown, in (b), the blocked faces are given colors corresponding to their blocking height.

Title Page

Abstract

Introduction

Conclusions

References

Tables

Figures

◀

▶

◀

▶

Back

Close

Full Screen / Esc

Printer-friendly Version

Interactive Discussion

